Preparation and properties of B4C-TiB2 ceramics prepared by spark plasma sintering

Jingzhe Fan
Zhengzhou University
Weixia Shen
Zhengzhou University
zhuangfei Zhang (zhangzf@zzu.edu.cn)
Zhengzhou University https://orcid.org/0000-0002-1148-0455
Chao Fang
Zhengzhou University
Yuewen Zhang
Zhengzhou University
Liangchao Chen
Zhengzhou University
Qianqian Wang
Zhengzhou University
Biao Wan
Zhengzhou University
Xiaopeng Jia
Zhengzhou University

Research Article

Keywords: Boron carbide ceramics, Conductivity, Hardness, Fracture toughness

Posted Date: September 28th, 2020

DOI: https://doi.org/10.21203/rs.3.rs-81425/v1

Dear Editor and Referees,

We would like to submit the enclosed manuscript entitled "**Preparation and properties of B_4C-TiB_2 ceramics prepared by spark plasma sintering**", which we wish to be considered for publication in **Journal of advanced ceramics**.

The paper is original and unpublished, and is not being or having been submitted for publication to any other journal, and that all the authors have read the paper and agree with its submission to **Journal of advanced ceramics**.

This manuscript was edited for proper English language, grammar, punctuation, spelling, and overall style by one or more of the highly qualified native English speaking editors at NativeEE. NativeEE specializes in editing and proofreading scientific manuscripts for submission to peer-reviewed journals.

The highlights are listed below:

- B_4C-TiB_2 can be synthesized with spark plasma sintering.
- TiH_2 contents can effectively increase the conductivity and the fracture toughness of B_4C.
- The electrical conductivity of 114.9 S/cm is obtained, which is 100% higher than that of B_4C.

I hope this paper is suitable for "**Journal of advanced ceramics**". We deeply appreciate your consideration of this manuscript.

Thank you and best regards.

Yours sincerely,

Zhuangfei Zhang and co-authors

School of Physics and Microelectronics, Zhengzhou University, Zhengzhou 450052, China

E-mail: zhangzf@zzu.edu.cn

Preparation and properties of B_4C-TiB_2 ceramics prepared by spark plasma sintering

Jingzhe Fan[a], Weixia Shen[a], Zhuangfei Zhang[a*], Chao Fang[a], Yuewen Zhang[a], Liangchao Chen[a*], Qianqian Wang[a], Biao Wan[a], Xiaopeng Jia [a*]

[a] Key Laboratory of Material Physics, Ministry of Education, School of Physics and Microelectronics, Zhengzhou University, Zhengzhou 450052, China.

Abstract: By doping titanium hydride (TiH_2) into boron carbide (B_4C), a series of B_4C + x wt% TiH_2 (x = 0, 5, 10, 15 and 20) composite ceramics were obtained through spark plasma sintering (SPS). The effects of sintering temperature and the amount of TiH_2 additive on the microstructure, mechanical and electrical properties of the sintered B_4C-TiB_2 composite ceramics were investigated. Powder mixtures of B_4C with 0–20 wt% TiH_2 were heated from 1400 to 1800 °C for 20 minutes under 50 MPa. The results indicated that higher sintering temperatures contributed to greater ceramic density. With increasing TiH_2 content, titanium diboride (TiB_2) formed between the TiH_2 and B_4C matrix. This effectively improved Young's modulus and fracture toughness of the composite ceramics, significantly improving their electrical properties: the electrical conductivity reached 114.9 $S \cdot cm^{-1}$ at 1800 °C when x = 20. Optimum mechanical properties were obtained for the B_4C ceramics sintered with 20 wt% TiH_2, which had a relative density of 99.9 ± 0.1%, Vickers hardness of 31.8 GPa and fracture toughness of 8.5 $MPa \cdot m^{1/2}$. The results indicated that the doping of fine Ti particles into the B_4C matrix increased the conductivity and the fracture toughness of B_4C.

Keywords: Boron carbide ceramics; Conductivity; Hardness; Fracture toughness;

1. Introduction

With developments in science and technology, the research and application of ceramic composite materials have attracted increasing attention. Furthermore, due to the electrical conductivity of ceramics, they can be widely used as high-temperature electrothermal elements in oxidising atmospheres, as cathodes in high-temperature fuel cells (HTFC) and as electrodes for magnetohydrodynamic (MHD) power generation[1-2]. Traditional conductive ceramic materials, whether oxide or non-oxide ceramic materials, have low conductivity at room temperature. Therefore, the synthesis of conductive super-hard materials at room temperature would not only be of great scientific significance but also of great value for expanding the applications of ceramic materials.

The third hardest material known to man, black diamond, or B_4C ceramic[3-4], is an attractive ceramic because of its excellent properties such as low density (2.51 $g \cdot cm^{-3}$), high melting point (2447 °C), high hardness (29–31 GPa), outstanding chemical stability and excellent absorption neutron cross-section (600 b). It has many applications, such as abrasive cutting, as a coating material, for light-weight armour and for controlling nuclear fission[5-6]. B_4C ceramic also has high Young's modulus (390–440 GPa) and low fracture toughness (2.16–2.52 $MPa \cdot m^{1/2}$)[7-8]. Due to these characteristics, B_4C ceramic is too difficult to sinter. However, B_4C ceramic with high density can be obtained by pressureless sintering (PS) or hot pressing (HP) at above 2200 °C, these conditions not only enable the grains to grow too easily but also waste

thermal energy, which greatly limits B_4C ceramic application[9-10].

TiB_2 is another super-hard material with high hardness (34 GPa) and superconductivity (14.4 μΩ·cm). It can be combined with B_4C to form a composite material that results in inhibition of grain growth, lower sintering temperature and improved mechanical properties[11-17]. When sintered at high temperature, the overall performance of nanoscale Ti and B_4C powders is weaker than that of pure B_4C[18]. Additionally, Ti is easily oxidised into Ti-O phase, or Ti-B-O and Ti-C-O solid solutions. Nanoscale Ti powers are usually unstable, so they are too difficult to handle. Therefore, TiH_2 has been used to disperse Ti particles in the B_4C ceramic matrix to synthesise TiB_2, thereby optimising its performance[19]. In addition, the fabrication of B_4C-TiB_2 composite ceramics using B_4C and TiH_2 as starting materials by the spark plasma sintering (SPS) method has not yet been reported. The main aim of the present work was to synthesise B_4C-TiB_2 composite ceramics and investigate the effect of TiH_2 powders on the B_4C ceramic properties.

2 . Materials and methods

B_4C powder (99.5%, 1–10 μm) and TiH_2 powder (99%, –325mesh) were purchased from Shanghai Aladdin Biochemical Technology, Shanghai, China and used as the starting materials[20]. Figure 1 shows the microstructures of these two raw materials. Powders composed of B_4C and TiH_2 (0, 5, 10, 15, 20 wt%) were mixed for more than 30 minutes in an agate mortar and then put into a graphite die (40 mm in depth and 13.1 mm in diameter). The die was lined with graphite paper to separate the powders from

graphite mould. The mixtures were sintered by SPS (LABOX-325R, Sinter Land Inc, Japan) under a uniaxial pressure of 50 MPa in a vacuum. A schematic diagram of the sample preparation process and SPS is shown in Figure 2. Using a two-stage heating process, TiH_2[21-23] was first completely decomposed at 800 °C for 10 minutes and then heated to 1400, 1500, 1600, 1700 and 1800 °C for 20 minutes, each, at a heating rate of 100 °C·min^{-1}. Figure 3 shows the temperature and displacement changes of the sample during 1800 °C sintering, revealing that the sample had a positive displacement and indicating that the sample was gradually densified.

After polishing the sintered B_4C-TiB_2 composite ceramics, their density was determined using the Archimedes displacement method. The microstructures of the composite ceramics were characterised by X-Ray diffraction (XRD; X-pert, Japan) using Cu-Ka radiation (λ=1.5418 Å) and scanning electron microscopy (SEM; JSM-IT200(A), Japan). The elemental analysis of the B_4C-TiB_2 composite ceramics was obtained by energy dispersive spectroscopy (EDS; JSM-IT200(A), Japan). The hardness of the B_4C-TiB_2 composite ceramics was measured by a Vickers hardness tester (KB5-BVZ, Germany) with an applied load of 0.1−5 N for 10 s on the polished surface. The electrical performance was measured by a Hall effect measurement system (ECOPIA/HMS-5500, Korea). The shear and longitudinal velocities were measured by an ultrasound measurement system (OWON, 5072PR, China) to calculate Young's modulus, and then fracture toughness was calculated based on indentation crack length.

3 . Results and discussion

3.1. Density and Phase compositions

The densities of B_4C + x wt% TiH_2 (x = 0, 5, 10, 15, 20) sintered at 1400, 1500, 1600, 1700 and 1800 °C are shown in Table 1. The results showed that the pure B_4C ceramic reached complete densification at 1800 ℃ (the theoretical density of B_4C is 2.51 $g \cdot cm^{-3}$). Figure 4 shows the density of B_4C ceramics sintered with different TiH_2 content at 1800 °C[24], with increasing TiH_2 content, the density of the composite ceramic reached a maximum at 20 wt% TiH_2. Both TiB_2 and C can reduce sintering temperature and inhibit grain growth. Because TiB_2 has relatively low crystalline boundary diffusion coefficient, which promotes slow densification[25], graphite (C) has a binding effect on grain boundary, which can enhance grain bounding diffusing and fast densification[26]. Therefore, the B_4C-TiB_2 composite ceramics are densified well.

Figure 5 shows the XRD analysis of the B_4C-TiB_2 composite ceramics doped with different TiH_2 content and sintered at 1800 °C for 20 minutes. With increasing TiH_2 content, the intensity of the TiB_2 diffraction peaks (around 44°) continued to increase and reached a maximum with 20 wt% TiH_2[27]. Due to the decomposition of TiH_2 powder at 620 °C via the process shown in Equation (1), the temperature was maintained at 800 °C for 10 minutes to ensure the complete formation of Ti. B_4C is divided into B and C through the process shown in Equation (2), the presence of element C in the XRD pattern also confirms this statement. Ti and B form TiB_2 through the process shown in Equation (3), The results indicated that an appropriate ratio of B_4C

and TiH_2 could be completely converted into B_4C-TiB_2 ceramics through the process shown in Equation (4) after sintering in SPS in a high vacuum environment. In this experiment, TiB_2 was generated by the in situ reaction of B_4C and TiH_2, which can be described by the following three equations:

$$TiH_2 \rightarrow Ti + H_2 \quad (1)$$

$$B_4C \rightarrow 4B + C \quad (2)$$

$$Ti + 2B \rightarrow TiB_2 \quad (3)$$

The overall reaction can be summarised as follows:

$$B_4C + 2TiH_2 = 2TiB_2 + C + 2H_2\uparrow \quad (4)$$

Figure 6 (a)–(f) shows images of the microstructure of B_4C-TiB_2 composite ceramics containing different TiH_2 content. The content of second-phase TiB_2 increased with increasing TiH_2 content. It was supposed that Ti originally existed at the brighter areas, and then the melted Ti reacted with B to form TiB_2 in situ during sintering. Grain growth was not obvious in the B_4C matrix as it was inhibited by the reaction of second-phase TiB_2. When the content of TiH_2 was increased to 20 wt%, large-sized TiB_2 grains of about 3–4 μm appeared with inhomogeneous distribution in the microstructure, as shown in Figure 6 (e), these could aggregate into 30–40 μm grains. The reaction between Ti and B is highly exothermic in behaviour and the heat generated helps to accelerate the formation of TiB_2 readily. The primary TiB_2 particles on the surface of B_4C are appreciably free and movable and because of boron diffusion across boundary layer, TiB_2 particles produces growth with the primary ones formed agglomerates[28].

Figure 7 shows the results of energy-dispersive X-ray spectroscopy (EDS) of part A in Figure 6 (f). Figure 7 (a) is an enlarged image of A, and the elemental content and distribution of A are shown in Figure 7 (b)–(f). XRD results combined with EDS spectra confirmed the phase distribution and that the light grey phase[29] was TiB_2, which has excellent electrical conductivity.

Figure 8 shows the EDS analysis of part B in Figure 6 (f). Figure 8 (a) is an enlarged image of B, and the elemental content and distribution of B are shown in Figure 8 (b)–(f). XRD results combined with EDS spectra confirmed that the phase distribution of the matrix was B_4C, which has poor electrical conductivity.

3.2. Hardness and fracture toughness

The mechanical properties of B_4C-TiB_2 were measured on the polished surface, as displayed in Figure 9 [30-31]. The hardness-load curve of B_4C–20 wt% TiH_2 is shown in Figure 9(a), revealing the obvious decrease in Vickers hardness (Hv) with increasing applied force, which was primarily attributed to the indentation size effect. An asymptotic Hv value of ~31.4 GPa was obtained when the applied load exceeded 5 N. It may be because the hardness of TiB_2 generated by the reaction is 34 GPa, and the hardness of C produced by the reaction is poor, which hardness is 1~2 GPa[32-33], the hardness of B_4C is 31 GPa, which hardness is between TiB_2 and C. However, the results indicate that due to very little C produced by the reaction, the hardness of B_4C-TiB_2 composite ceramics does not decrease under the combined action of TiB_2 and C. Vickers hardness and fracture toughness results for the B_4C-TiB_2 composite ceramics are shown

in Figure 9(b). When doped with 20 wt% TiH_2, the hardness of the sample was stable and the fracture toughness was a maximum of 8.5 $MPa \cdot m^{1/2}$. TiB_2 is a high-toughness material, and C also can be used as an additive to produce high-toughness ceramic[34-37], so the fracture toughness of B_4C-TiB_2 composite ceramics are improved.

To calculate fracture toughness, an oscilloscope was used to measure the shear and longitudinal wave sound velocities and then the Poisson ratio μ was calculated using Equation (5). Data for the Young's modulus calculation was then obtained using Equation (6). Finally, the fracture toughness of the B_4C-TiB_2 composite ceramics was calculated according to Equation (7).

The crack trace of the polished surface of the 20 wt% TiH_2 composite ceramic is shown in Figure 10. Crack bridging, crack deflection, crack bending and crack forking occurred when force was applied, and these cracks acted as toughening for consuming energy. Crack bridging is helpful to improve fracture toughness[38]. The following three formulas were applied to calculate fracture toughness:

$$\mu = \frac{\frac{1}{2}(\frac{V_L}{V_T})^2 - 1}{(\frac{V_L}{V_T})^2 - 1} \tag{5}$$

$$E = \frac{V_L^2 \times \rho \times (1-\mu) \times (1-2\mu)}{1-\mu} \tag{6}$$

$$K_{IC} = 0.016 \times (\frac{E}{H_V})^{\frac{1}{2}} \times \frac{P}{C^{\frac{3}{2}}} \tag{7}$$

3.3. Electrical conductivity

The electrical conductivity of the B_4C + x wt% TiH_2 (x = 0, 5, 10, 15, 20) composite

ceramics at different sintering temperatures (1400, 1500, 1600, 1700 and 1800 °C) is shown in Figure 11. The electrical conductivity could be enhanced by increasing the sintering temperature and increasing the content of TiH_2. When doped with 5 wt% or 10 wt% TiH_2, the electrical conductivity of the B_4C-TiB_2 composite ceramics suddenly increased. When TiH_2 was further increased to 15 wt% or 20 wt%, the electrical conductivity of the B_4C-TiB_2 composite ceramics was two orders of magnitude higher than that of pure B_4C. At room temperature, a maximum electrical conductivity of 114.9 $S \cdot cm^{-1}$ was achieved with 20 wt% TiH_2. Graphite is one type of carbon-based filler, due to being layered structure, its electrical conductivity is 10^4 S/cm at room temperature[39]. Ti reacted with B to form TiB_2, the layered structure of boron atoms similar to graphite and the outer electrons of Ti determine the outstanding electrical conductivity of TiB_2, they can be used for improving the electrical conductivity of composite ceramics.

4. Conclusions

Completely densified B_4C-TiB_2 composite ceramics with high conductivity, high strength and high hardness properties were successfully obtained by the spark plasma sintering method starting from raw mixtures of B_4C and TiH_2 powders. Using TiH_2 as a sintering aid improved the density of the B_4C ceramics. During the sintering process, B_4C reacted with Ti to form TiB_2 and a small amount of C, which successfully inhibited the growth of B_4C and improved the electrical conductivity, Young modulus and fracture toughness.

Acknowledgements

This work was supported by the National Natural Science Foundation of China (No. 11704340 and 11804305), and The Scientific and Technology project in Henan Province (No. 202102210198).

References

[1] An LQ, Wang LY, Wang LF, Fan RH, Ito A, Goto T. Fabrication of $Lu_2Ti_2O_7$-Lu_3NbO_7 solid solution transparent ceramics by spark plasma sintering and their electrical conductivities. J Eur Ceram Soc 2020, 40: 4589-4594. https://doi.org/10.1016/j.jeurceramsoc.2020.05.008.

[2] Grigoriev SN, Volosova MA, Peretyagin PY, Seleznev AE, Okunkova AA, Smirnov A. The effect of TiC additive on mechanical and electrical properties of Al_2O_3 ceramic. Appl Sci-Basel 2018, 8: 2385-8387. https://doi.org/10.3390/app8122385.

[3] Domnich V, Reynaud S, Haber RA, Chhowalla M. Boron Carbide: Structure, Properties, and Stability under Stress. J Am Ceram Soc 2011, 94: 3605-3628. https://doi.org/10.1111/j.1551-2916.2011.04865.x.

[4] Jamale S, Kumar BVM. Sintering and sliding wear studies of B_4C-SiC composites. Int J Refract Met H 2020, 87: 105124. https://doi.org/10.1016/j.ijrmhm.2019.105124.

[5] He Y, Shen YD, Tang B, An Q. Enhanced strength and ductility of superhard boron carbide through injecting electrons. J Eur Ceram Soc 2020, 40: 4428-4435. https://doi.org/10.1016/j.jeurceramsoc.2020.06.004.

[6] Zhang W, Yamashita S, Kita H. Progress in pressureless sintering of boron carbide

ceramics-a review. ADV Appl Ceram 2019, 118: 222-239. https://doi.org/10.1080/17436753.2019.1574285.

[7] Badica P, Grasso S, Borodianska H, Xie SS, Li PF, Takarko P, Reece MJ, Sakka Y, Vasylkiv O. Tough and dense boron carbide obtained by high-pressure (300 MPa) and low-temperature (1600 °C) spark plasma sintering. J Ceram Soc Jpn 2014, 122: 271-275. https://doi.org/10.2109/jcersj2.122.271.

[8] K. Sairam, J.K. Sonber, T.S.R.C. Murthy, C. Subramanian, R.K. Fotedar, P. Nanekar, R.C. Hubli, Influence of spark plasma sintering parameters on densification and mechanical properties of boron carbide, Int. J. Refract. Met. H. 42 (2014) 182-192. https://doi.org/10.1016/j.ijrmhm.2013.09.004.

[9] Singh P, Singh B, Kumar M, Kumar A. One step reduction of Boric Acid to boron carbide nanoparticles. Ceram Int 2014, 40: 15331-15334. https://doi.org/10.1016/j.ceramint.2014.06.101.

[10] Moskovskikh DO, Paramonov KA, Nepapushev AA, Shkodich NF, Mukasyan AS. Bulk boron carbide nanostructured ceramics by reactive spark plasma sintering. Ceram Int 2017, 43: 8190-8194. https://doi.org/ 10.1016/j.ceramint.2017.03.145.

[11] Heydari MS, Baharvandi HR. Comparing the effects of different sintering methods for ceramics on the physical and mechanical properties of B_4C–TiB_2 nanocomposites. Int J Refract Met H 2015, 51: 224-232. https://doi.org/10.1016/j.ijrmhm.2015.04.003.

[12] Heydari MS, Baharvandi HR. Effect of different additives on the sintering ability and the properties of B_4C-TiB_2 composites. Int J Refract Met H 2015, 51: 61-69.

https://doi.org/10.1016/j.ijrmhm.2015.02.014.

[13] White RM, Dickey EC. Mechanical properties and deformation mechanisms of B_4C-TiB_2 eutectic composites. J Eur Ceram Soc 2014, 34: 2043-2050. https://doi.org/10.1016/j.jeurceramsoc.2013.08.012.

[14] Gao YB, Tang TG, Yi CH, Zhang W, Li DC, Xie WB, Huang W, Ye N. Study of static and dynamic behavior of TiB_2–B_4C composite. Mater Design 2016, 92: 814-822. https://doi.org/10.1016/j.matdes.2015.12.123.

[15] He QL, Wang AY, Liu C, Wang WM, Wang H, Fu ZY. Microstructures and mechanical properties of B_4C-TiB_2-SiC composites fabricated by ball milling and hot pressing. J Eur Ceram Soc 2018, 38: 2832-2840. https://doi.org/10.1016/j.jeurceramsoc.2018.02.020.

[16] Yue XY, Zhao SM, Lu P, Chang Q, Ru HQ. Synthesis and properties of hot pressed B_4C–TiB_2 ceramic composite. Mat Sci Eng A-Struct 2010, 527: 7215-7219. https://doi.org/10.1016/j.msea.2010.07.101.

[17] White RM, Kunkle JM, Polotai AV, Dickey EC. Microstructure and hardness scaling in laser-processed B_4C–TiB_2 eutectic ceramics. J Eur Ceram Soc 2011, 31: 1227-1232. https://doi.org/10.1016/j.jeurceramsoc.2010.06.013.

[18] Karimoto T, Nishimoto A. Simultaneous Boronizing and Carburizing of Titanium via Spark Plasma Sintering. Mater Trans 2019, 60: 2387-2391. https://doi.org/10.2320/matertrans.L-M2019838.

[19] Shi SF, Cho SH, Goto T, Sekino T. Fine Ti-dispersed Al_2O_3 composites and their

mechanical and electrical properties. J Am Ceram Soc 2018, 101: 3181-3190. https://doi.org/10.1111/jace.15472.

[20] Tan YQ, Chen C, Li FZ, Zhang HB, Zhang GJ, Peng SM. Enhancement of sinterability and mechanical properties of B_4C ceramics using Ti_3AlC_2 as a sintering aid. RSC Adv 2015, 5: 76309-76314. https://doi.org/10.1039/c5ra14191e.

[21] Pan Y, Chen S. Exploring the novel structure, transportable capacity and thermodynamic properties of TiH_2 hydrogen storage material. Int J Energ Res 2020, 44: 4997-5007. https://doi.org/10.1002/er.5260.

[22] Ito M, Setoyama D, Matsunaga J, Muta H, Kurosaki K, Uno M, Yamanaka S. Electrical and thermal properties of titanium hydrides. J Alloy Compd 2006, 420: 25-28. https://doi.org/10.1016/j.jallcom.2005.10.032.

[23] Liu H, He P, Feng JC, Cao J. Kinetic study on nonisothermal dehydrogenation of TiH_2 powders. Int J Hydrogen Energ 2009, 34: 3018-3025. https://doi.org/10.1016/j.ijhydene.2009.01.095.

[24] Rehman SS, Ji W, Khan SA, Fu ZY, Zhang F. Microstructure and mechanical properties of B_4C densified by spark plasma sintering with Si as a sintering aid. Ceram Int 2015, 41: 1903-1906. https://doi.org/10.1016/j.ceramint.2014.09.115.

[25] Pei LZ, Xiao HN. B_4C/TiB_2 composite powders prepared by carbothermal reduction method. J Mater Process Tech 2009, 209: 2122-2128. https://doi.org/10.1016/j.jmatprotec.2008.05.003.

[26] Yin BY, Wang LS, Fang YC. Sintering mechanism of pure and carbon-doped boron

carbide. J Chin Ceram Soc 2001, 29: 68-71. https://doi.org/10.14062/j.issn.0454-5648.2001.01.015.

[27] Yin SP, Zhang ZH, Cheng XW, Su TJ, Hu ZY, Song Q, Wang H. Spark plasma sintering of B_4C-TiB_2-SiC composite ceramics using B_4C, Ti_3SiC_2 and Si as starting materials. Ceram Int 2018, 44: 21626-21632. https://doi.org/10.1016/j.ceramint.2018.08.245.

[28] Suresh S, Moorthi NSV. Aluminium- titanium diboride (Al-TiB2) metal matrix composites: challenges and opportunities. Procedia Eng 2012, 38: 89–97. https://doi.org/10.1016/j.proeng.2012.06.013.

[29] Wen Q, Tan YQ, Zhong ZH, Zhang HB, Zhou XS. High toughness and electrical discharge machinable B_4C-TiB_2-SiC composites fabricated at low sintering temperature. Mat Sci Eng A-Struct 2017, 701: 338-343. https://doi.org/10.1016/j.msea.2017.06.100.

[30] Anstis GR, Chantikui P, Lawn BR, Marshall DB. A critical evaluation of indentation techniques for measuring fracture toughness: 1. direct crack measurements. J Am Ceram Soc 1981, 64: 533-538. https://doi.org/ 10.1111/j.1151-2916.1981.tb10320.x.

[31] Ma DJ, Wang JL, Sun L. Methodology for measuring fracture toughness of ceramic materials by instrumented indentation test with vickers indenter. J Am Ceram Soc 2017, 100: 2296-2308. https://doi.org/10.1111/jace.14650.

[32] Sengupta R, Bhattacharya M, Bandyopadhyay S, Bhowmick AK. A review on the mechanical and electrical properties of graphite and modified graphite reinforced

polymer composites. Prog Polym Sci 2011, 36: 638-670. https://doi.org/10.1016/j.propolymsci.2010.11.003.

[33] Oku T, Kurumada A, Imamura Y, Ishihara M. Effects of ionirradiation on the hardness properties of graphites and C/C composites by indentation tests. J Mucl Mater 2008, 381: 92-97. https://doi.org/10.1016/j.jnucmat.2008.07.026.

[34] Peng C, Tang H, He Y, Lu XQ, Jia P, Liu GY, Zhao YC, Wang MZ. A novel non-stoichiometric medium-entropy carbide stabilized by anion vacancies. J Mater Sci Technol 2020, 51: 161-166. https://doi.org/10.1016/j.jmst.2020.02.049.

[35] Skorokhod V, Krstic V. High strength-high toughness B_4C-TiB_2 composites. J Mater Sci Lett 2000, 19: 237-9. https://doi.org/10.1023/A:1006766910536.

[36] Shi L, Li HY, Zou ZM, Fok ASL, Marsden BJ, Hodgkins A, Mummery PM, Marrow J. Analysis of crack propagation in nuclear graphite using three-point bending of sandwiched specimens. J Nucl Mater 2008, 372: 141-151. https://doi.org/10.1016/j.jnucmat.2007.02.012.

[37] Chen HHN, Su RKL, Fok SL, Zhang HG. Fracture behavior of nuclear graphite under three-point bending tests. Eng Fract Mech 2017, 186: 143-157. https://doi.org/10.1016/j.engfracmech.2017.09.030.

[38] Ouagne P, Neighbour GB, McEnaney B. Crack growth resistance in nuclear graphites. J Phys D: Appl Phys 2002, 35: 927-934. https://doi.org/10.1088/0022-3727/35/9/315.

[39] Reis JML, Martins SA, Mattos HSD. Combination of temperature and electrical

conductivity on semiconductor graphite/epoxy composites. J Braz Soc Mech Sci 2020, 42: 8. https://doi.org/10.1007/s40430-020-02487-z.

Temperature(℃)	0wt%	5wt%	10wt%	15wt%	20wt%
1400	2.20	1.83	1.85	2.04	2.06
1500	2.23	2.12	2.03	2.34	2.28
1600	2.27	2.25	2.17	2.54	2.51
1700	2.42	2.36	2.51	2.59	2.52
1800	2.51	2.57	2.62	2.74	2.83

Table. 1. Density of monolithic B_4C sintered from 1400 ℃ to 1800 ℃.

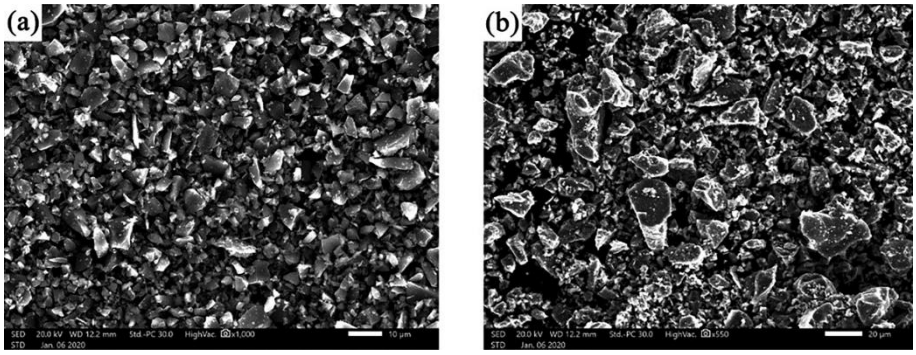

Fig.1. Microstructure of (a) B_4C and (b) TiH_2 powders.

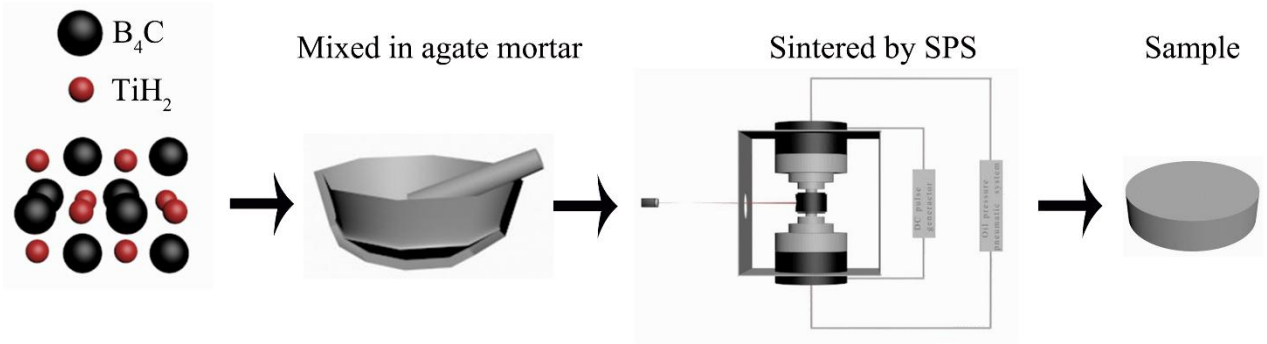

Fig.2. The procedure of sample sintering.

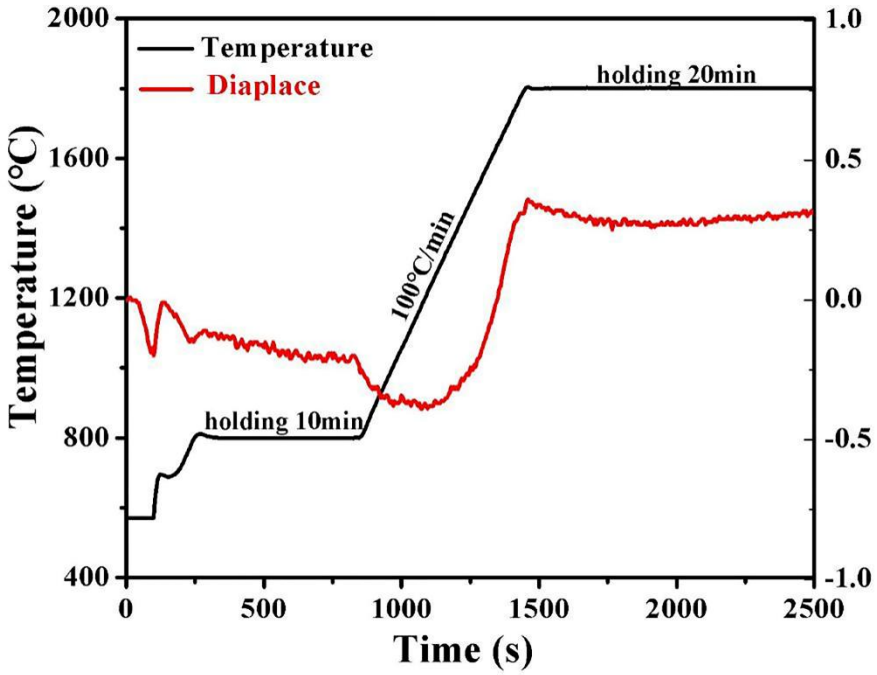

Fig.3. The temperature and displacement change at 1800 ℃ with SPS.

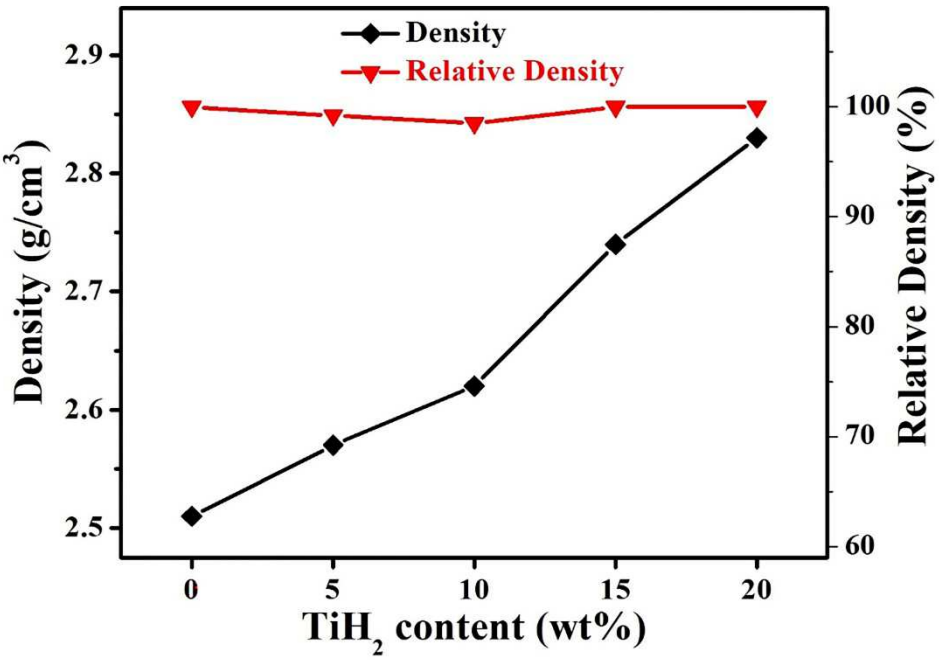

Fig. 4. Density of B_4C specimens as a function of (0-20) wt% TiH_2 content at 1800 ℃.

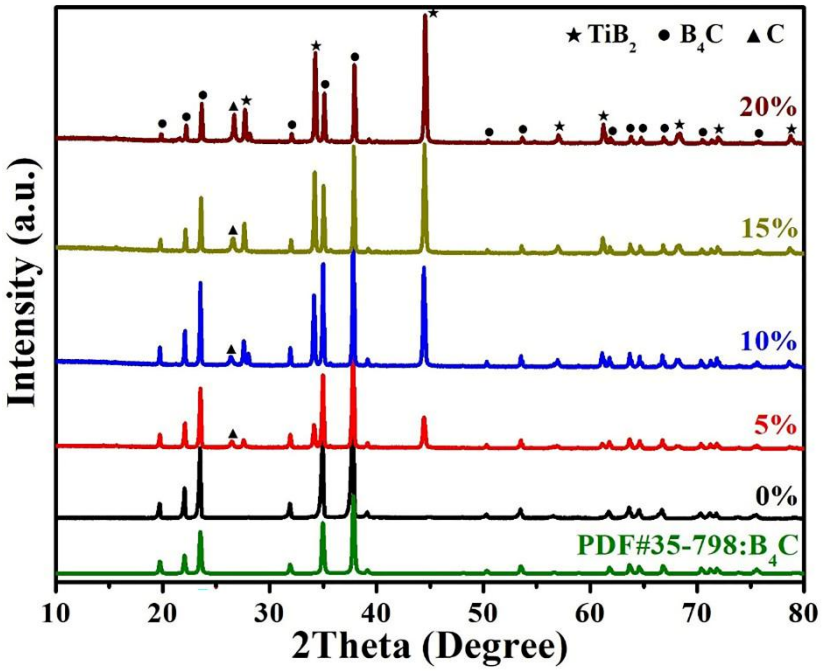

Fig.5. XRD patterns of the synthesized B_4C+x wt% TiH_2 (x=0, 5, 10, 15, 20) composite ceramics.

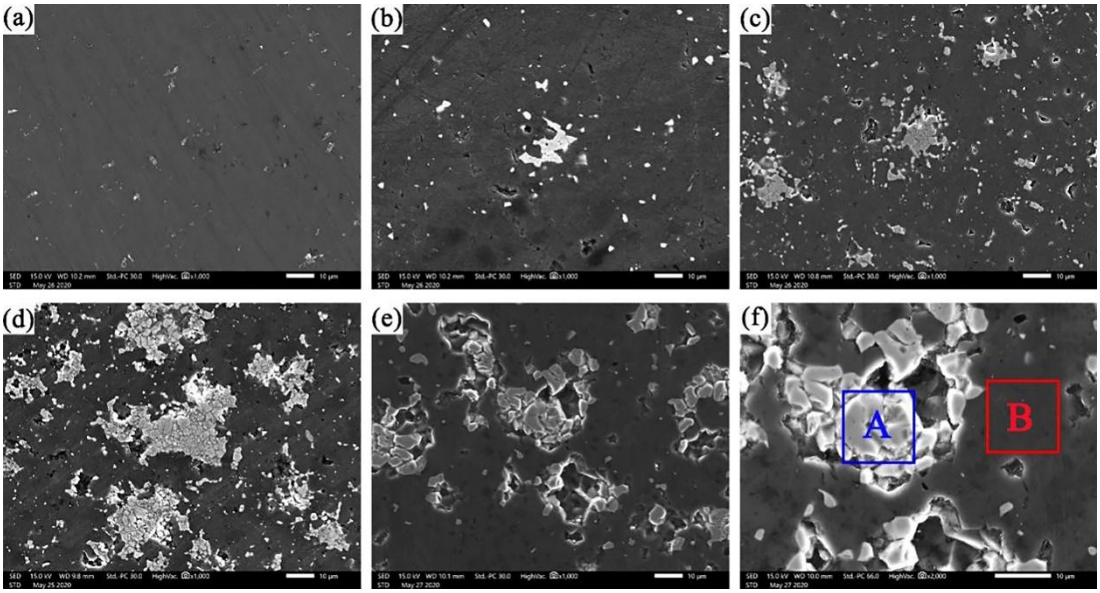

Fig.6. Polished surfaces of B_4C ceramics sintered with different amount of TiH_2 content sintered at 1800 ℃. (a) B_4C-0 wt% TiH_2; (b) B_4C-5 wt% TiH_2; (c) B_4C-10 wt% TiH_2; (d) B_4C-15 wt% TiH_2; (e) B_4C-20 wt% TiH_2; (f) The enlarged view of B_4C-20 wt% TiH_2.

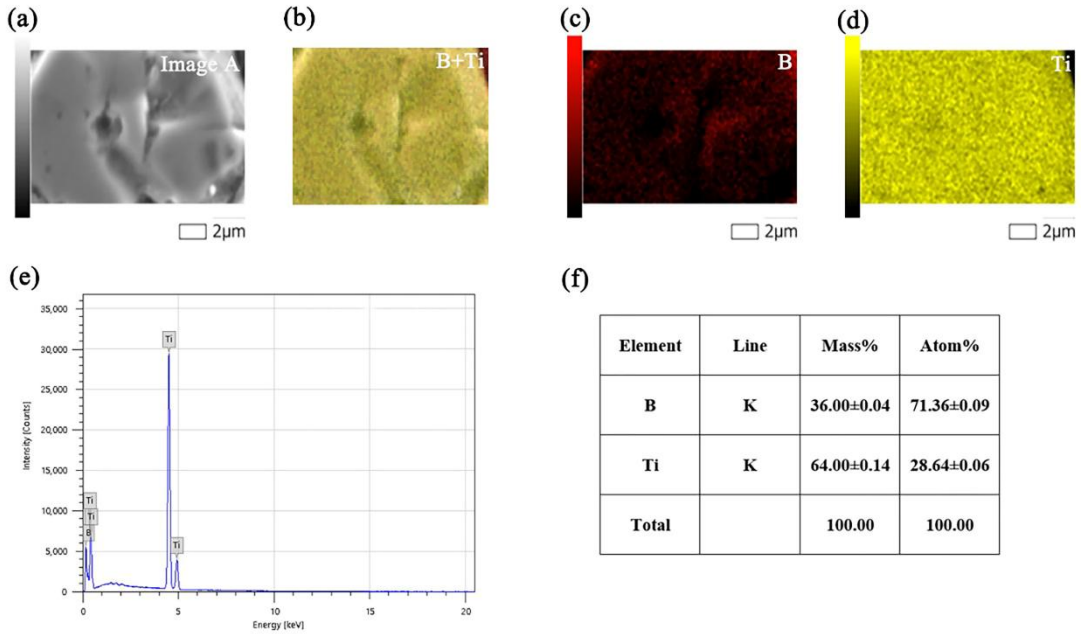

Element	Line	Mass%	Atom%
B	K	36.00±0.04	71.36±0.09
Ti	K	64.00±0.14	28.64±0.06
Total		100.00	100.00

Fig.7. The related EDS spectra of A sintered with 20wt% of TiH_2 content sintered at 1800 ℃. (a) EDS test area image A; (b) Ti-K,B-K; (c)B-K; (d)Ti-K; (e) EDS spectra of image A; (f) Element content of image A.

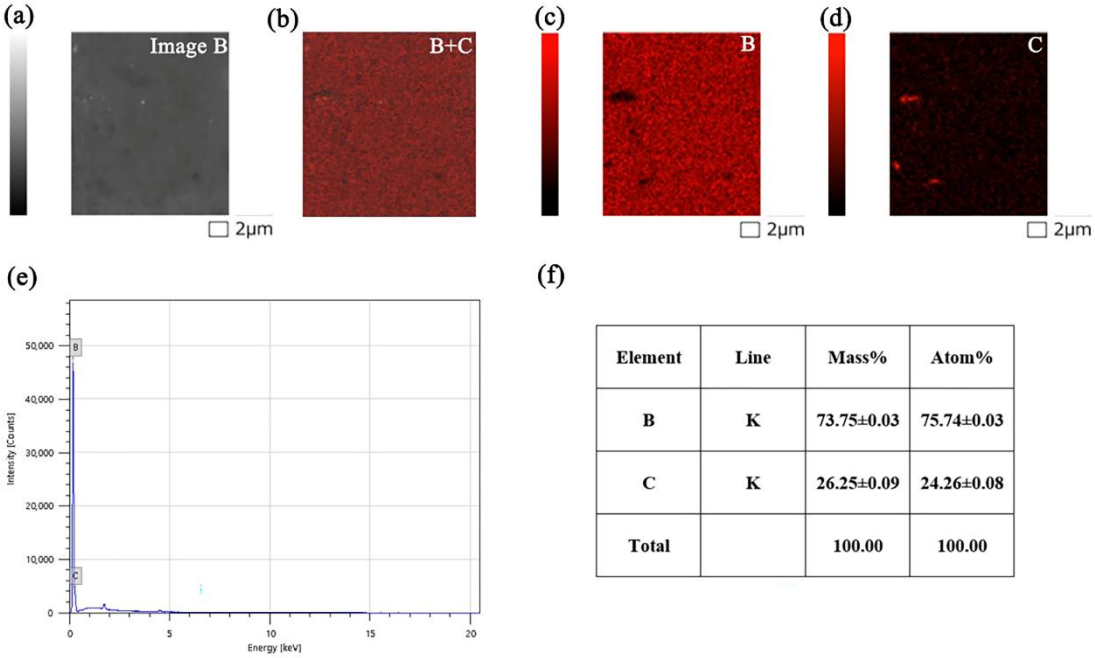

Element	Line	Mass%	Atom%
B	K	73.75±0.03	75.74±0.03
C	K	26.25±0.09	24.26±0.08
Total		100.00	100.00

Fig.8. The related EDS spectra of B sintered with 20wt% of TiH_2 content sintered at 1800 ℃. (a) EDS test area image B; (b) B-K,C-K; (c)B-K; (d) C-K; (e) EDS spectra of image B; (f) Element content of image B.

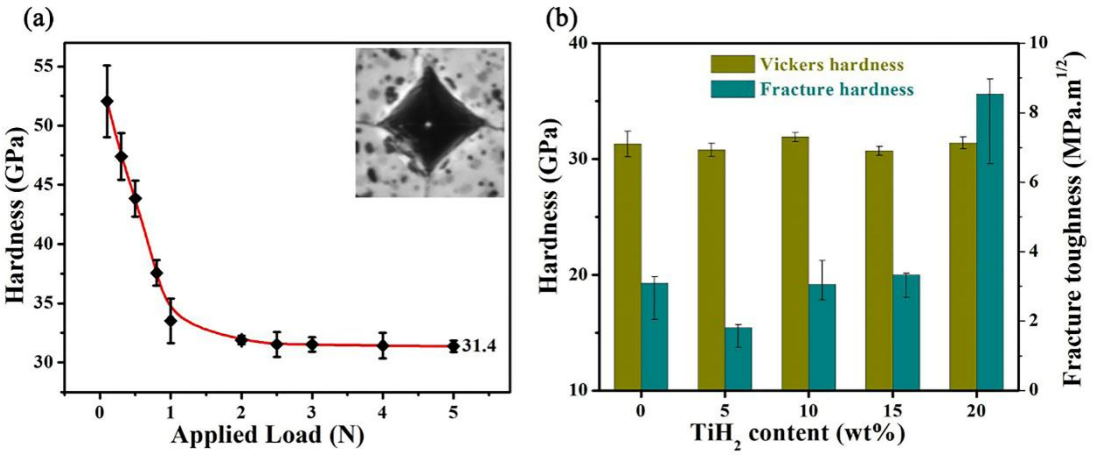

Fig. 9. Comparison of mechanical properties. (a) The measured Vickers hardness of B_4C-20 wt% TiH_2 under 5 N load at 1800 ℃. (b) Effect of TiH_2 addiction on the hardness and fracture toughness of B_4C at 1800 ℃.

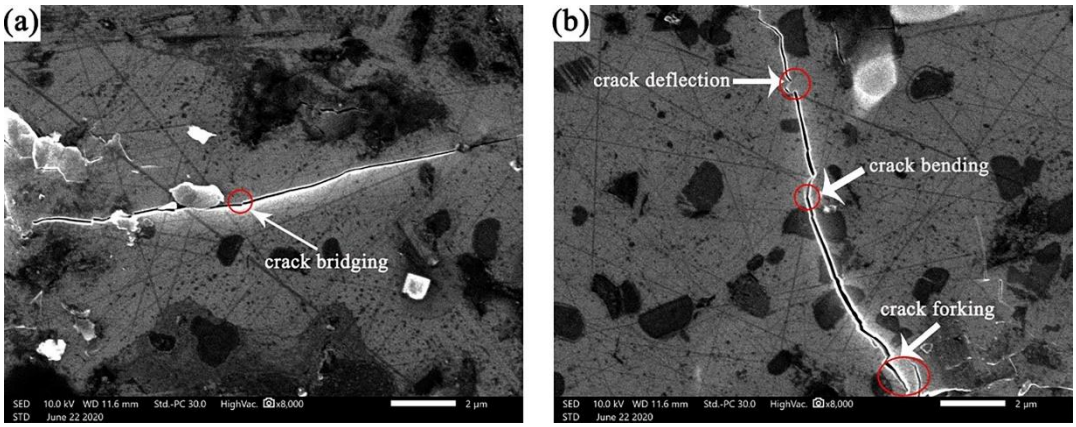

Fig.10. SEM micrographs of the polished surfaces cracks of the B_4C-TiB_2 composite ceramics with 20 wt% TiH_2.

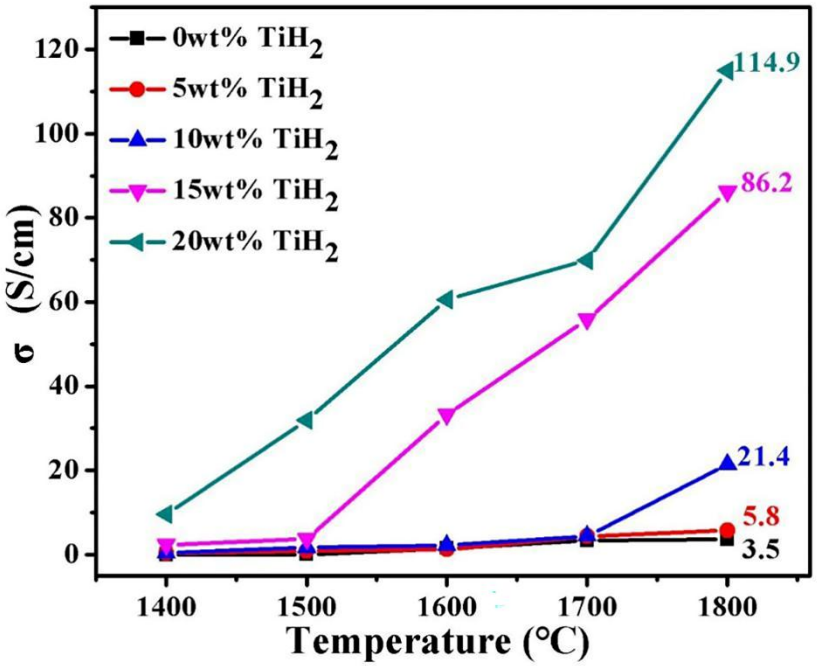

Fig. 11. The electrical conductivity of B_4C-(0, 5, 10, 15, 20) wt% TiH_2 composite ceramics at different sintering temperature.

Figures

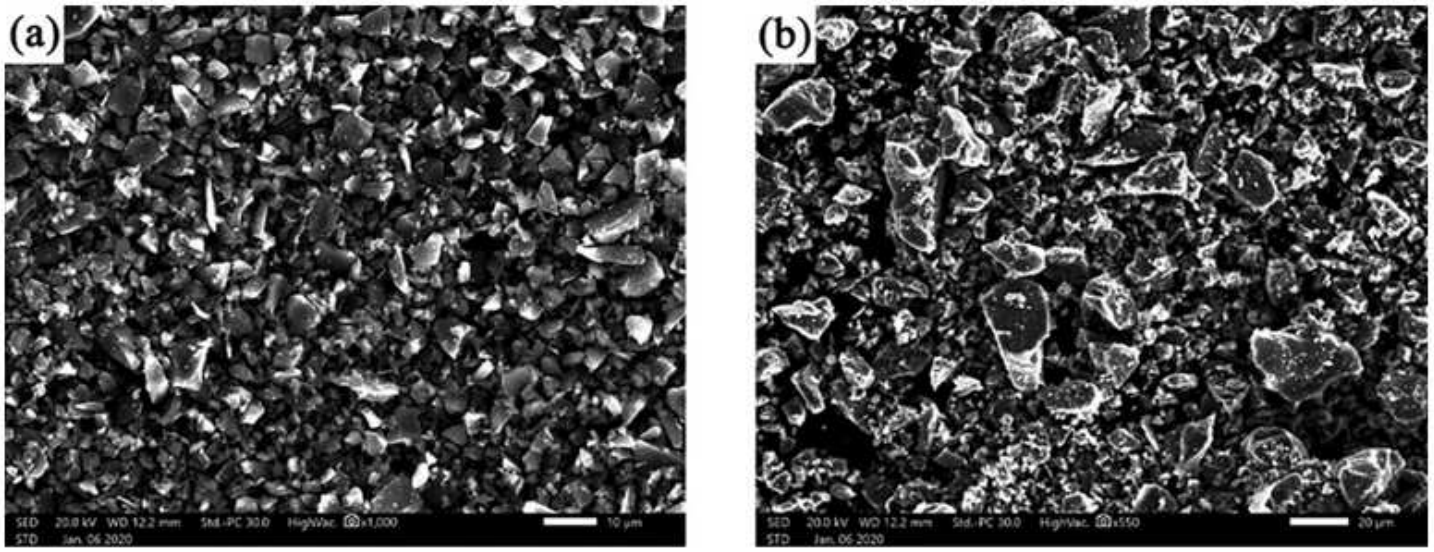

Figure 1

Microstructure of (a) B4C and (b) TiH2 powders.

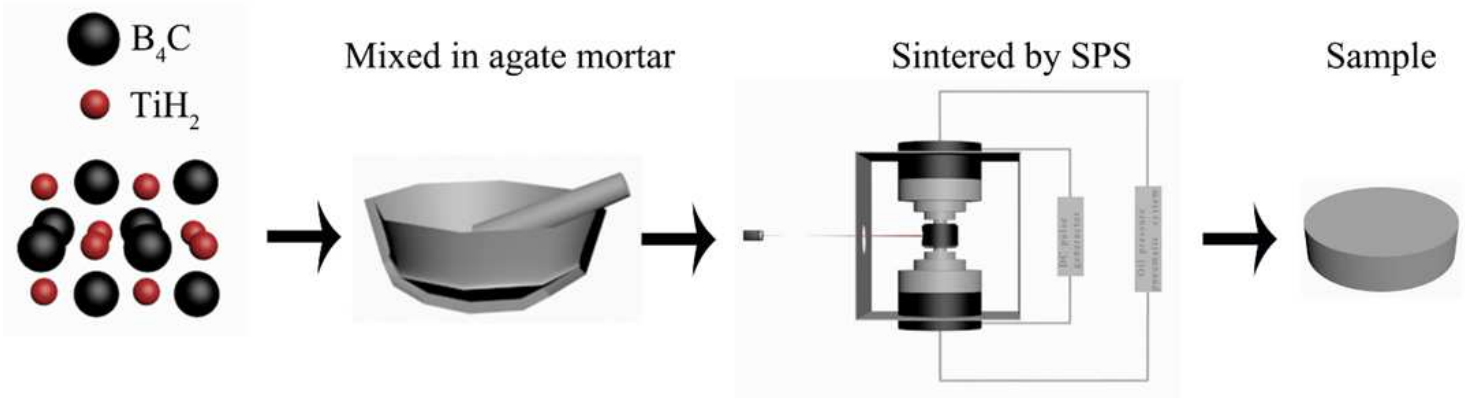

Figure 2

The procedure of sample sintering.

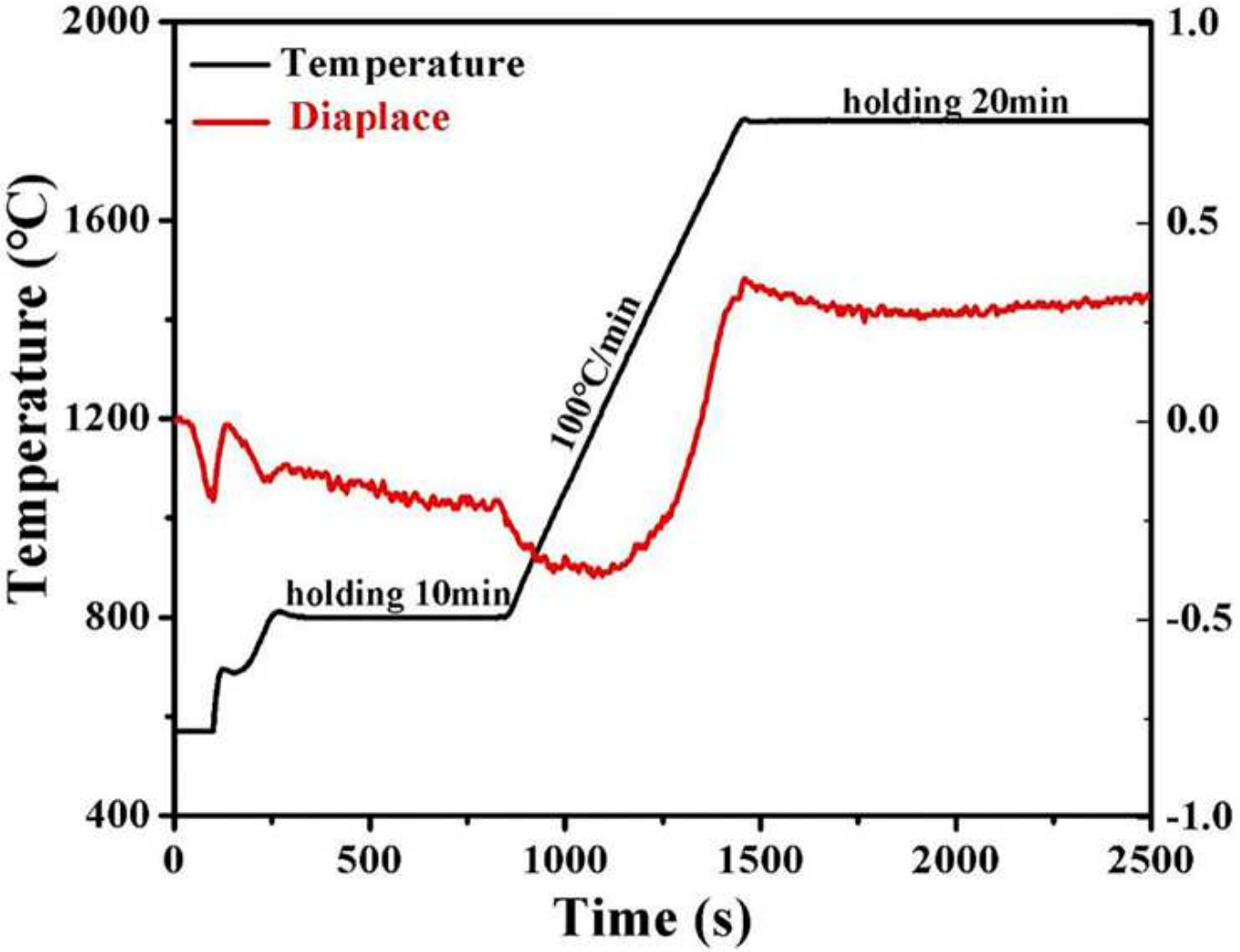

Figure 3

The temperature and displacement change at 1800 ℃ with SPS.

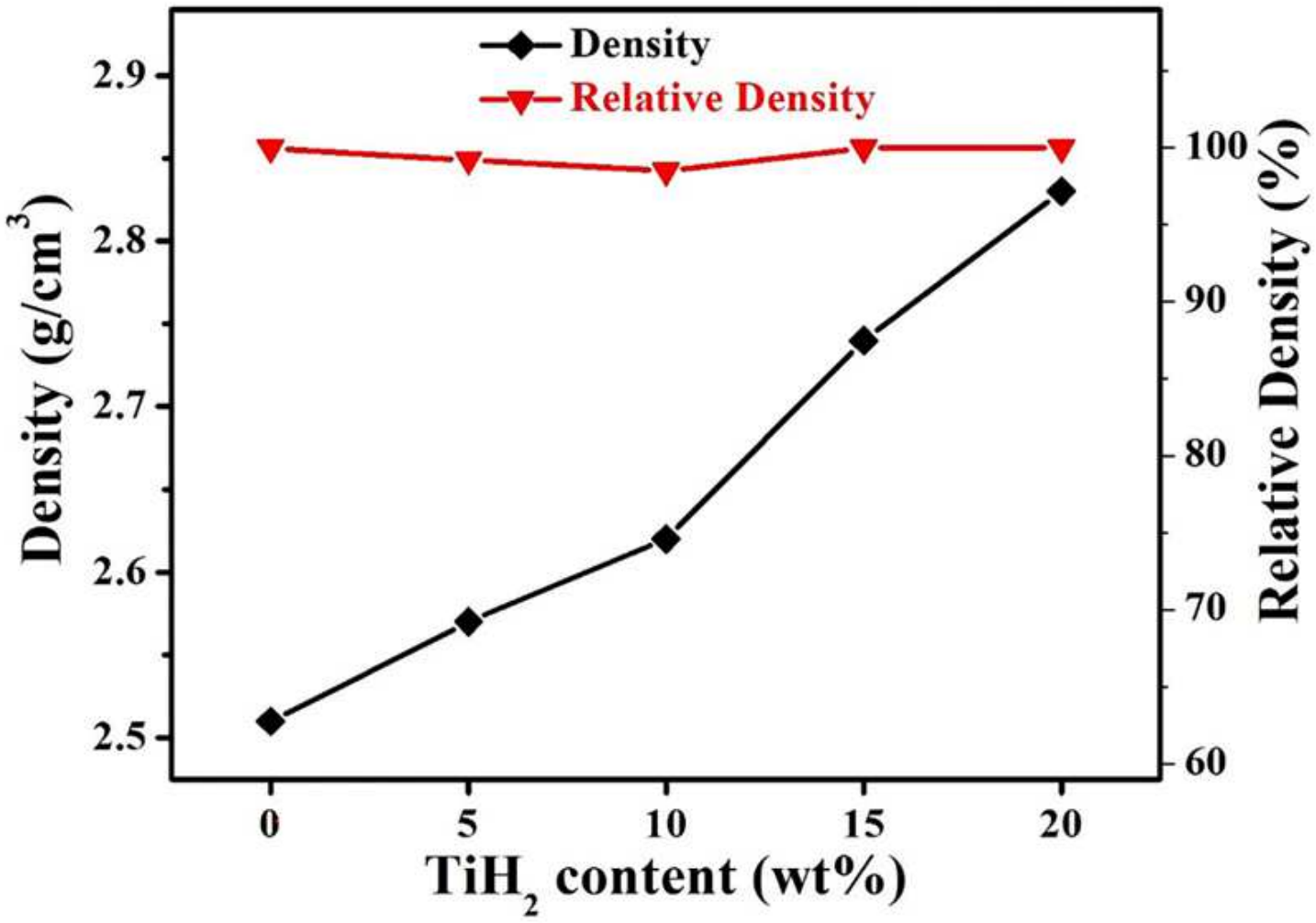

Figure 4

Density of B4C specimens as a function of (0-20) wt% TiH2 content at 1800 ℃.

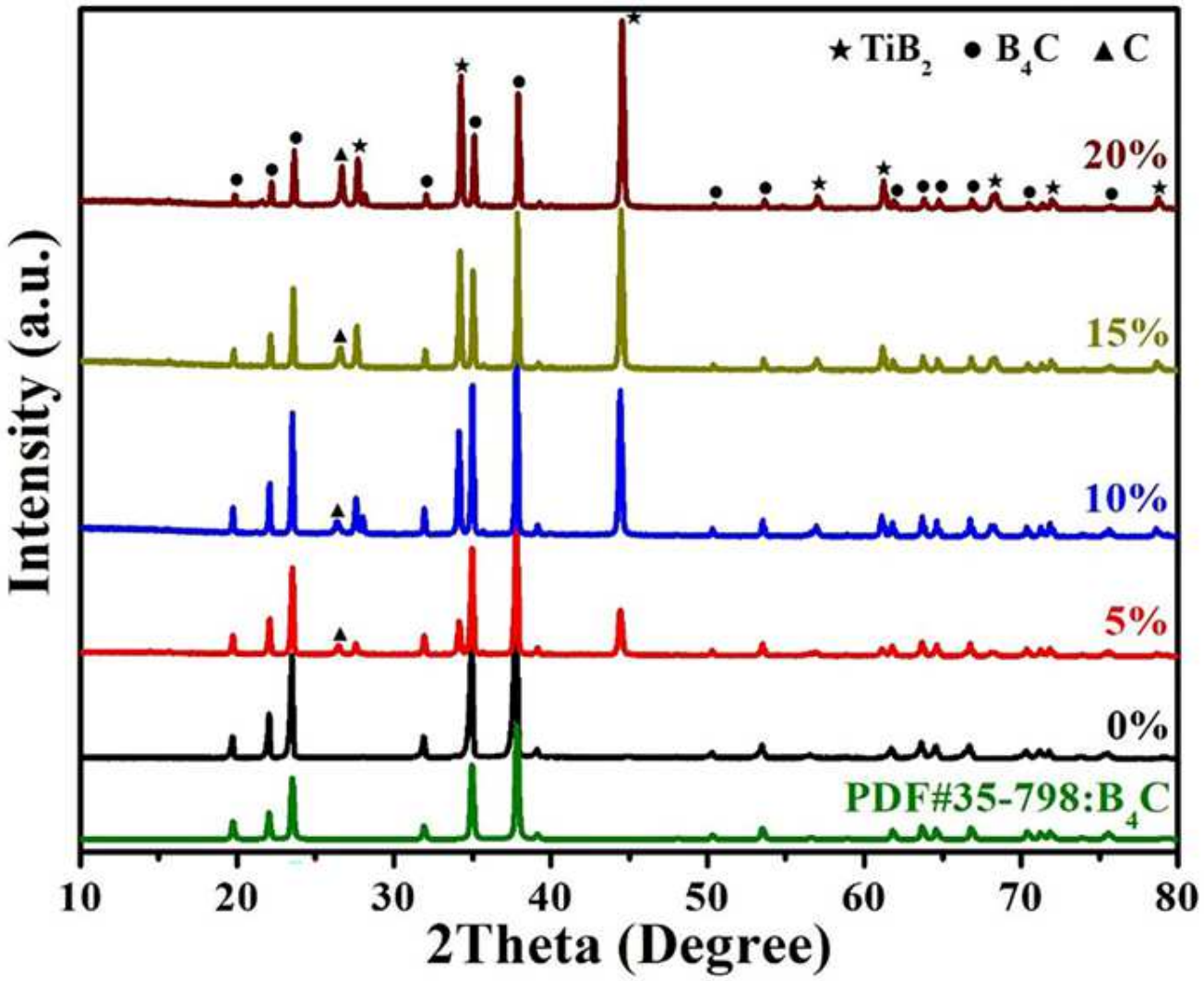

Figure 5

XRD patterns of the synthesized B4C+x wt% TiH2 (x=0, 5, 10, 15, 20) composite ceramics.

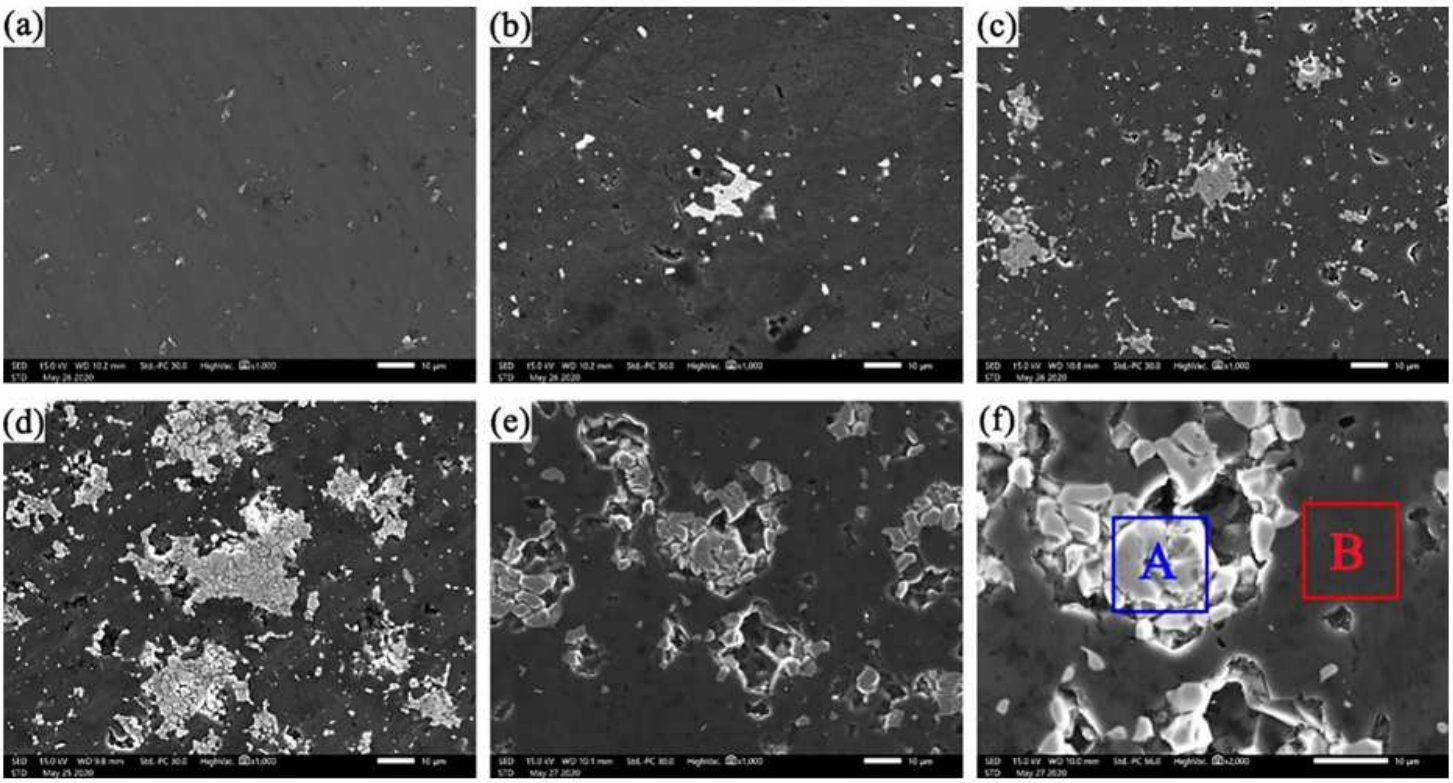

Figure 6

Polished surfaces of B4C ceramics sintered with different amount of TiH2 content sintered at 1800 ℃. (a) B4C-0 wt% TiH2; (b) B4C-5 wt% TiH2; (c) B4C-10 wt% TiH2; (d) B4C-15 wt% TiH2; (e) B4C-20 wt% TiH2; (f) The enlarged view of B4C-20 wt% TiH2.

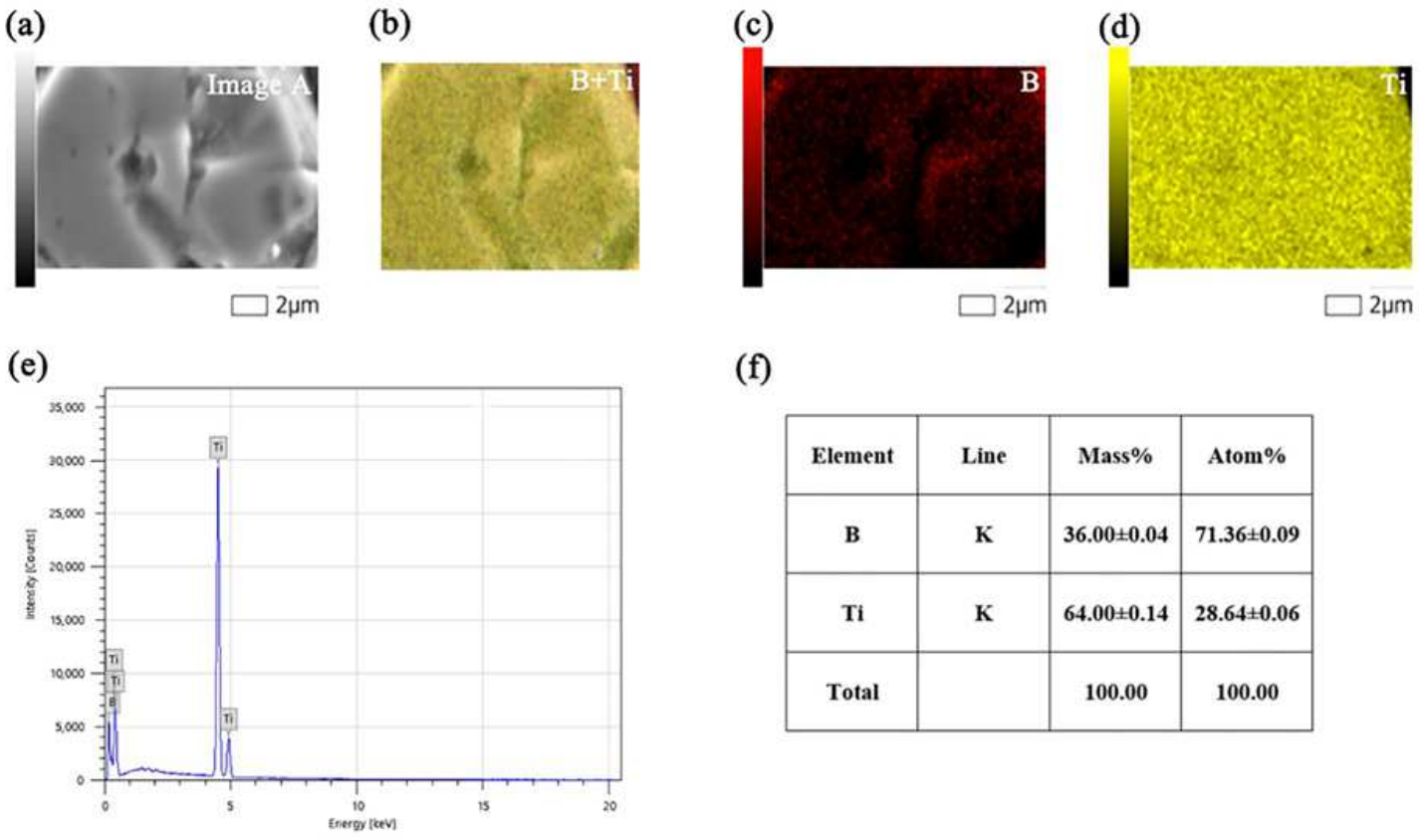

Element	Line	Mass%	Atom%
B	K	36.00±0.04	71.36±0.09
Ti	K	64.00±0.14	28.64±0.06
Total		100.00	100.00

Figure 7

The related EDS spectra of A sintered with 20wt% of TiH2 content sintered at 1800 ℃. (a) EDS test area image A; (b) Ti-K,B-K; (c)B-K; (d)Ti-K; (e) EDS spectra of image A; (f) Element content of image A.

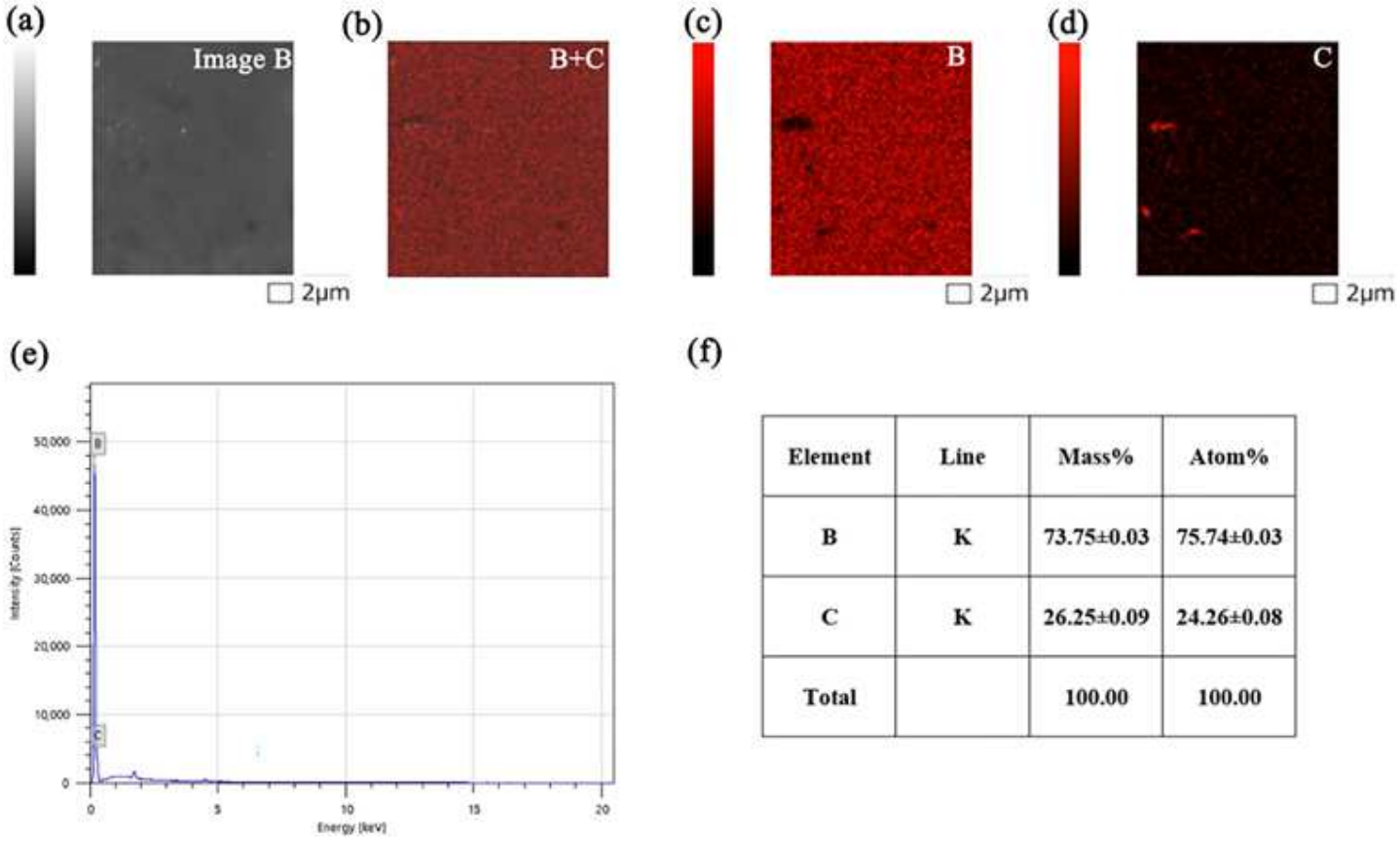

Element	Line	Mass%	Atom%
B	K	73.75±0.03	75.74±0.03
C	K	26.25±0.09	24.26±0.08
Total		100.00	100.00

Figure 8

The related EDS spectra of B sintered with 20wt% of TiH2 content sintered at 1800 ℃. (a) EDS test area image B; (b) B-K,C-K; (c)B-K; (d) C-K; (e) EDS spectra of image B; (f) Element content of image B.

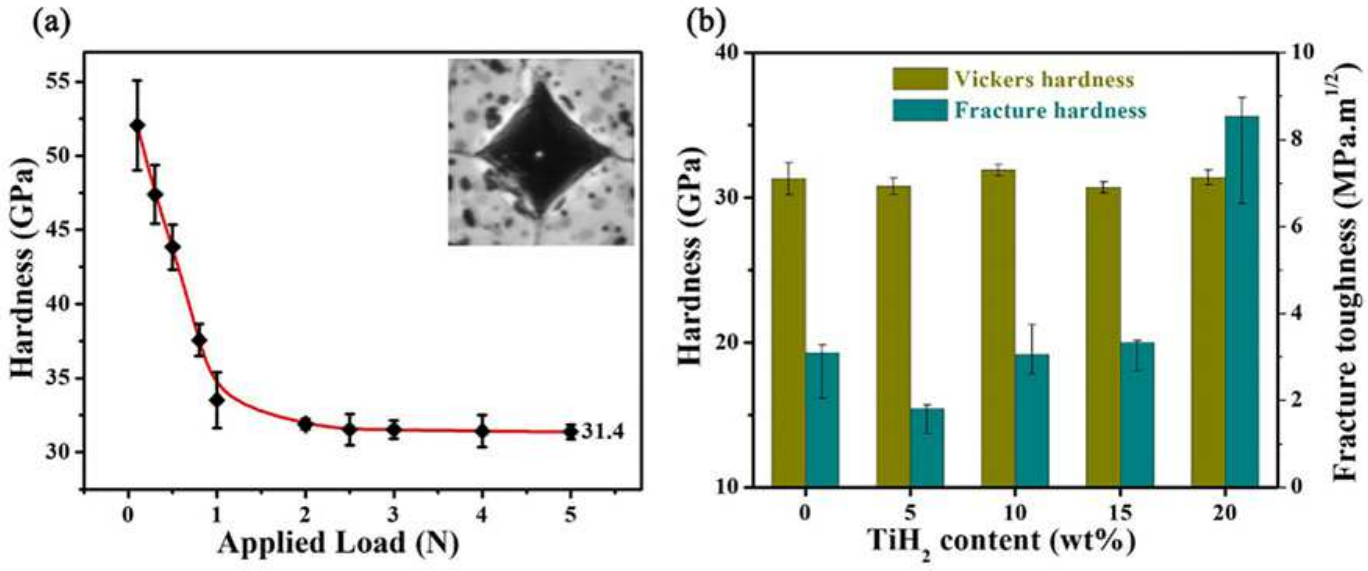

Figure 9

Comparison of mechanical properties. (a) The measured Vickers hardness of B4C-20 wt% TiH2 under 5 N load at 1800 □. (b) Effect of TiH2 addiction on the hardness and fracture toughness of B4C at 1800 □.

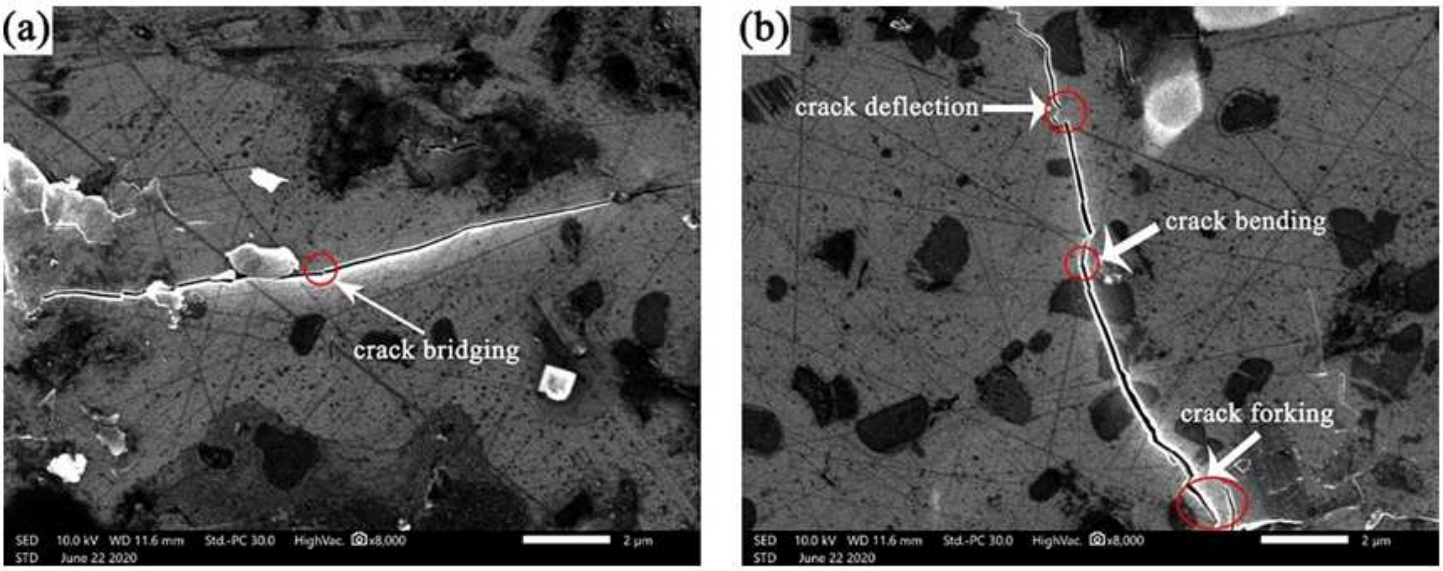

Figure 10

SEM micrographs of the polished surfaces cracks of the B4C-TiB2 composite ceramics with 20 wt% TiH2.

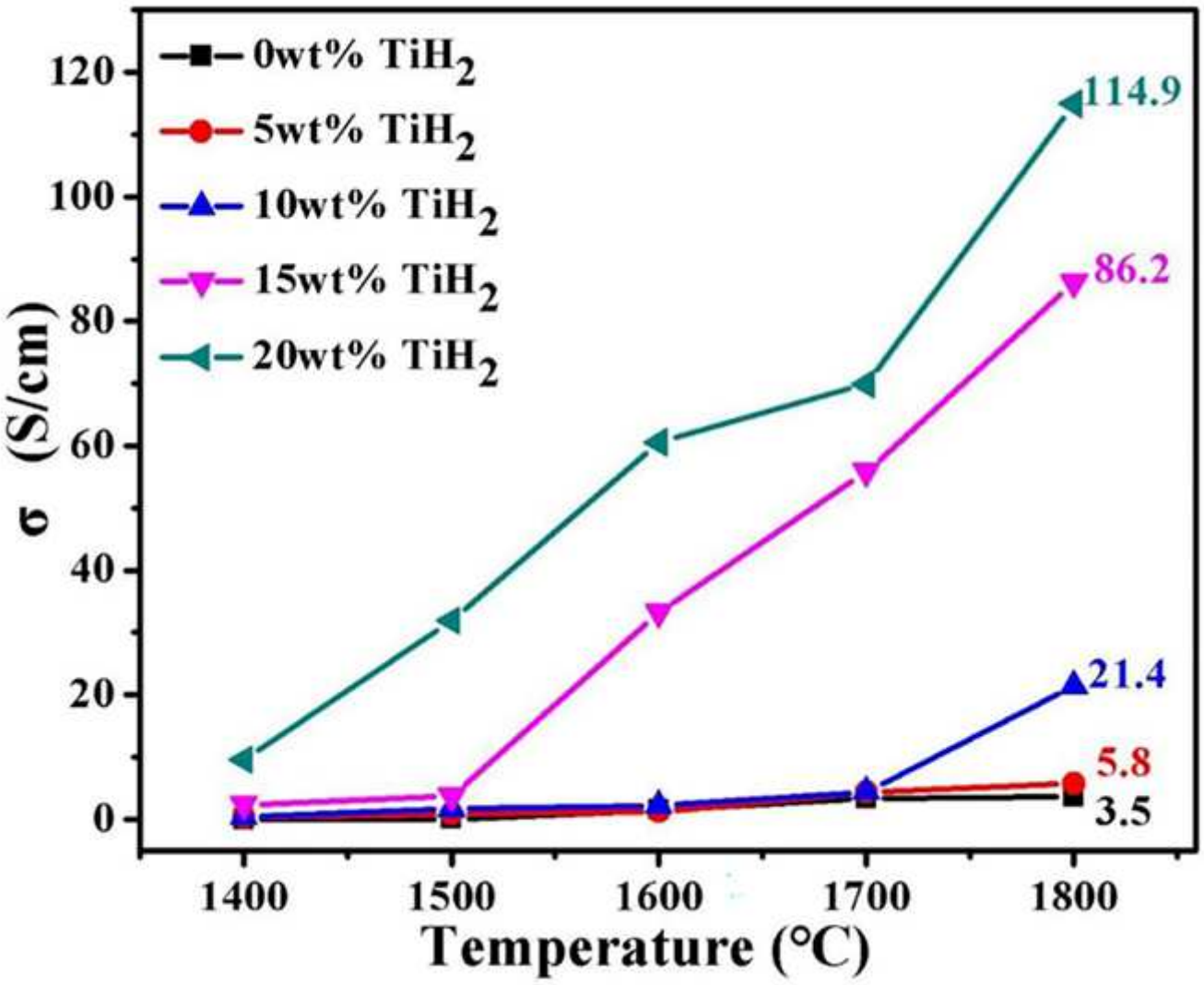

Figure 11

The electrical conductivity of B4C-(0, 5, 10, 15, 20) wt% TiH2 composite ceramics at different sintering temperature.